

Higher-Order Structure of Hamiltonian Truncation Effective Theory

Andrea Maestri,^{1, 2, *} Simone Rodini,^{1, 2, †} and Barbara Pasquini^{1, 2, ‡}

¹*Dipartimento di Fisica “A. Volta”, Università degli Studi di Pavia, I-27100 Pavia, Italy*

²*Istituto Nazionale di Fisica Nucleare, Sezione di Pavia, I-27100 Pavia, Italy*

(Dated: February 16, 2026)

We study the Hamiltonian truncation for the two-dimensional $\lambda\phi^4$ theory within the framework of Hamiltonian truncation effective theory, where truncation artifacts are mitigated through a systematic inclusion of corrective terms organized in inverse powers of the ultraviolet energy cut-off E_{\max} . Building on the leading-order matching program, we develop two complementary extensions. First, we derive compact all-order expressions for the local matching corrections to the mass and quartic coupling by resumming infinite classes of diagrams sharing fixed topologies within the local approximation. Second, we extend the non-local sector by computing the next-to-next-to-local corrections contributing at $\mathcal{O}(E_{\max}^{-4})$, following a continuum-first matching procedure, in which the effective corrections are computed in infinite volume and the spatial direction is subsequently recompactified to obtain a separable Hilbert-space basis on which the truncated operator construction is implemented. Our results show that an increasingly rich operator basis is necessary to describe the theory beyond leading order.

I. INTRODUCTION

Quantum field theory (QFT) provides the conceptual framework underlying the Standard Model, whose perturbative predictions have been tested with high precision across a wide range of energies. Many phenomena of interest in fundamental and many-body systems are, however, intrinsically non-perturbative. Some examples include confinement and the generation of mass gaps in non-abelian gauge theories, real-time dynamics in strongly correlated or out-of-equilibrium settings, and strongly coupled renormalization group flows [1–4]. In such regimes, the canonical perturbative expansion, for instance in terms of Feynman diagrams, is not reliable, and non-perturbative methods are required.

A standard non-perturbative route is the Euclidean lattice path-integral formulation, whose Monte Carlo evaluation has enabled first-principles results for a broad class of observables in strongly interacting theories [5]. Lattice Monte Carlo, however, is not universally applicable. In particular, finite-density systems and many real-time observables are affected by sign problems, which significantly restrict the practical use of importance-sampling techniques [6, 7]. These considerations have prompted the development of complementary approaches that are formulated directly in a Hamiltonian and/or real-time framework, including the Hamiltonian lattice formulation [8], tensor-network methods [9, 10], and quantum-simulation inspired strategies [11, 12].

Within this context, Hamiltonian truncation (HT) methods have attracted renewed attention. In these approaches, the full QFT Hamiltonian is approximated by restricting it to a finite-dimensional subspace of the Hilbert space and subsequently diagonalizing the resulting matrix. This approach originates in the truncated conformal space approach, introduced by Yurov and Zamolodchikov [13, 14], and it has since been developed along several directions. These include applications to a broad class of two-dimensional quantum field theories, such as the Ising model, the sine-Gordon and massive Schwinger models, as well as gauge theories defined on an interval [15–17]. Extensions to higher spacetime dimensions have also been explored, see for example Refs. [18, 19], as well as formulations in boosted frames [20].

Hamiltonian-truncation approaches have also been pursued in light-cone and conformal bases, where infinite-volume dynamics can be accessed efficiently within certain classes of models, see Refs. [21, 22]. Across these various implementations, a common practical challenge is the rapid growth of the truncated basis with the energy cut-off E_{\max} . This growth leads to an exponential increase in computational cost and complicates simple expectations for the scaling of truncation errors, thereby motivating the development of renormalized and improved variants of HT, in which the effects of high-energy states are systematically integrated out rather than simply discarded [18, 23–28].

In parallel, alternative directions have been explored to mitigate the computational cost associated with large Hilbert spaces. One such direction is the use of Hamiltonian-truncation bases as qubit-efficient encodings for digital quantum simulations of real-time QFT dynamics and scattering processes [29, 30].

* Electronic address: andrea.maestri01@universitadipavia.it

† Electronic address: simone.rodini@unipv.it

‡ Electronic address: barbara.pasquini@unipv.it

Another complementary approach is provided by Hamiltonian truncation effective theory (HTET), introduced in Ref. [31] and developed further in the subsequent works [32–34], which treat the cut-off E_{\max} as an effective field theory (EFT) scale. States above E_{\max} are integrated out, yielding a finite-dimensional effective Hamiltonian acting on the truncated subspace. Corrections are organized as a controlled expansion in inverse powers of E_{\max} , with an interplay between local terms and genuinely non-local contributions.

In this work we further develop the HTET program along two main directions. First, building on Ref. [31], we develop an all-order resummation of the local HTET contributions, with the aim of improving the practical convergence of the effective Hamiltonian at fixed computational cost. Second, extending Ref. [32], we derive the second-order non-local corrections and reformulate the matching directly in the continuum, postponing space compactification. This reorganization makes the structure of the expansion more transparent and facilitates higher-order computations.

The paper is organized as follows. In Sec. II we review HT and its EFT reformulation, introducing the truncation via an energy cut-off E_{\max} and defining the truncated effective Hamiltonian. We then specialize to two-dimensional $\lambda\phi^4$ theory as a testing model, detailing the construction of the Fock basis and the implementation of the truncation scheme.

In Sec. III we develop the resummation of local terms, by summing together infinite classes of diagrams that share a fixed topology. The sums are performed to all orders and within the local approximation, yielding compact expressions for the matching corrections to the mass and quartic coupling. In Sec. IV we derive the next-to-next-to-local (NNLO) corrections, extending the systematic $1/E_{\max}$ expansion and formulating the matching directly in the continuum to handle the associated distributional structures. Finally, in Sec. V we present a numerical analysis of the resulting effective Hamiltonians, assessing the impact of the resummed and NNLO contributions on the convergence of low-energy spectral observables.

II. HAMILTONIAN TRUNCATION EFFECTIVE THEORY FOR THE $\lambda\phi^4$ THEORY IN TWO DIMENSIONS

In this section, we briefly introduce the HT method [13, 14, 18], and its formulation as HTET [31], in the case of the two-dimensional $\lambda\phi^4$ theory defined on a circle of circumference $L = 2\pi R$. The basic idea is to map an infinite-dimensional problem into a finite-dimensional numerical one by restricting the space of states to those with energies below an ultraviolet (UV) cut-off E_{\max} , while systematically controlling the truncation errors.

One starts by splitting the full Hamiltonian into a free, solvable part and an interaction term,

$$H = H_0 + V, \quad (1)$$

with H_0 such that its spectrum and eigenstates are exactly known, i.e.,

$$H_0 |\mathcal{E}_i\rangle = \mathcal{E}_i |\mathcal{E}_i\rangle, \quad \langle \mathcal{E}_i | \mathcal{E}_j \rangle = \delta_{ij}. \quad (2)$$

The strategy is then to numerically diagonalize the full Hamiltonian H in the basis of eigenstates of H_0 , with the aim of extracting eigenvalues and eigenvectors defined by $H|\Psi\rangle = E|\Psi\rangle$. This requires making the Hilbert space \mathcal{H} , spanned by the free eigenstates, finite dimensional. To this end, one first compactifies the spatial dimensions, so that the spectrum of H_0 becomes discrete and the Hilbert space separable. One then introduces an energy cut-off E_{\max} on the free spectrum, which induces an orthogonal decomposition of \mathcal{H} into low-energy and high-energy subspaces, i.e.,

$$\mathcal{H} = \mathcal{H}_{\text{tru}} \oplus \mathcal{H}_{\text{neg}}, \quad \mathcal{H}_{\text{tru}} = \text{span}\{|\mathcal{E}_i\rangle : \mathcal{E}_i \leq E_{\max}\}, \quad \mathcal{H}_{\text{neg}} = \text{span}\{|\mathcal{E}_i\rangle : \mathcal{E}_i > E_{\max}\}. \quad (3)$$

By construction, \mathcal{H}_{tru} is finite-dimensional and therefore suitable for numerical analysis. It is then convenient to introduce the following projection operators

$$P \doteq \sum_{E_i \leq E_{\max}} |\mathcal{E}_i\rangle\langle\mathcal{E}_i|, \quad Q \doteq \sum_{E_i > E_{\max}} |\mathcal{E}_i\rangle\langle\mathcal{E}_i|, \quad P + Q = \mathbb{1}. \quad (4)$$

HT, hereafter referred to as “raw”, corresponds to simply approximating the full Hamiltonian as $H \simeq PHP$. The accuracy of this approximation improves as a power law in E_{\max} . However, the computational cost required to achieve this improvement grows rapidly with the size of the basis, since the number of states included in \mathcal{H}_{tru} scales exponentially with E_{\max} .

Several methods have been developed to mitigate this problem by improving the convergence, see Refs. [24–28]. HTET is one such approach, in which an EFT framework is employed to systematically improve the accuracy of the truncation. The key observation is that, for sufficiently large E_{\max} , the UV dynamics associated with highly energetic states can be treated perturbatively, while the numerical diagonalization on \mathcal{H}_{tru} captures the non-perturbative physics

in the infrared (IR) sector. This is precisely the setting in which the EFT viewpoint becomes natural, since the effects of the excluded states in \mathcal{H}_{neg} can be absorbed into effective operators acting within the truncated theory.

HTET provides a systematic framework for this procedure by constructing an effective Hamiltonian $H_{\text{eff}} = H_0 + V_{\text{eff}}$ defined on \mathcal{H}_{tru} , where

$$V_{\text{eff}} = H_1 + H_2 + H_3 + \dots, \quad H_n = \mathcal{O}(V^n). \quad (5)$$

The effective Hamiltonian H_{eff} is obtained operationally by requiring that a low-energy observable agrees between the fundamental theory and the effective theory defined at the scale E_{max} . The chosen observable is the transition matrix T , defined from the time-evolution operator in the interaction picture and admitting a perturbative expansion in V . Let $|i\rangle$ and $|f\rangle$ denote low-energy external states, with $\mathcal{E}_{i,f} \ll E_{\text{max}}$, and introduce the energy differences

$$E_{fi} \doteq \mathcal{E}_f - \mathcal{E}_i, \quad E_{f\alpha} \doteq \mathcal{E}_f - \mathcal{E}_\alpha, \quad (6)$$

where \mathcal{E}_α is the energy of an intermediate state $|\alpha\rangle$. By imposing the equality between the fundamental and effective transition matrices order by order in V , one obtains matching conditions for the operators H_n . At the lowest orders, these read

$$\langle f | H_1 | i \rangle_{\text{eff}} = \langle f | V | i \rangle, \quad (7)$$

$$\langle f | H_2 | i \rangle_{\text{eff}} = \sum_{\alpha}^{\geq} \frac{\langle f | V | \alpha \rangle \langle \alpha | V | i \rangle}{\mathcal{E}_{f\alpha}}, \quad (8)$$

where the notation \sum_{α}^{\geq} indicates that the sum over intermediate states is restricted to those satisfying $\mathcal{E}_\alpha > E_{\text{max}}$.

To quantify the corrections to H_{eff} from Eq. (8), we consider the two-dimensional $\lambda\phi^4$ theory, defined by a quartic self-interaction with coupling constant λ and a mass parameter m . Despite its simplicity, this model captures all the structural features relevant for HT.

In two dimensions, the scalar field has scaling dimension $[\phi] = 0$, while the mass and the quartic coupling have mass dimensions $[m^2] = [\lambda] = 2$. As a consequence, the interaction is strongly relevant, in the sense that its coupling has positive mass dimension and therefore grows rapidly toward the IR. This also implies that the UV behavior of the theory is particularly well controlled once normal ordering is imposed.

In finite volume, one works with the so-called “naive” Hamiltonian

$$H = H_0 + V = \sum_k \omega_k a_k^\dagger a_k + \frac{\lambda}{4!} \int_0^L dx : \phi^4(x) :, \quad L = 2\pi R. \quad (9)$$

More precisely, one should account for Casimir-energy contributions and for terms arising from the mismatch between normal ordering defined at finite volume and in the infinite-volume limit. These effects are, however, exponentially suppressed in the regime $Lm \gg 1$.

To discretize the spectrum of H_0 and obtain a countable basis, the theory is defined on a cylinder $S_R^1 \times \mathbb{R}$ with periodic boundary conditions, $\phi(x + 2\pi R, t) = \phi(x, t)$. The compactification discretizes the momentum modes and allows for a Fourier expansion. For a massive scalar field, one can write

$$\phi(x, t) = \frac{1}{\sqrt{2\pi R}} \sum_{k \in \mathbb{Z}} \frac{1}{\sqrt{2\omega_k}} \left(a_k e^{-ikx/R} + a_k^\dagger e^{ikx/R} \right), \quad \omega_k = \sqrt{(k/R)^2 + m^2}, \quad (10)$$

with $[a_k, a_{k'}^\dagger] = \delta_{kk'}$. It is convenient to introduce positive and negative frequency components, corresponding to annihilation and creation operators:

$$\phi_k = \phi_k^{(+)} + \phi_{-k}^{(-)}, \quad \phi_k^{(+)} = \frac{1}{\sqrt{2\omega_k}} a_k, \quad \phi_k^{(-)} = \frac{1}{\sqrt{2\omega_k}} a_k^\dagger. \quad (11)$$

The eigenstates of H_0 are Fock states, labeled by occupation numbers $n_k \in \mathbb{N}_0$,

$$|\bar{n}\rangle \doteq |n_0, n_1, n_{-1}, \dots\rangle = \prod_{k \in \mathbb{Z}} \frac{(a_k^\dagger)^{n_k}}{\sqrt{n_k!}} |0\rangle, \quad H_0 |\bar{n}\rangle = \left(\sum_k \omega_k n_k \right) |\bar{n}\rangle. \quad (12)$$

Having established the truncated basis and the operator setup, we now turn to the explicit determination of the HTET matching corrections in the 2d $\lambda\phi^4$ theory. In the local approximation, the matching corrections can then be represented as a finite set of local operators (counterterms) acting within \mathcal{H}_{tru} , with coefficients that depend on E_{max} but not on the external energies. Beyond this leading order, the matching acquires a residual dependence on $\mathcal{E}_{i,f}$, and the corrections can no longer be represented purely in terms of local operators. These genuinely non-local contributions are, however, parametrically suppressed by additional powers of $1/E_{\text{max}}$.

III. RESUMMATION OF LOCAL EXPANSION

Reference [31] carries out the matching procedure described in Sec. II explicitly up to order $\mathcal{O}(V^2)$ using a diagrammatic approach. This analysis yields local corrections to the quartic coupling and to the mass, which significantly improve the convergence of Hamiltonian-truncation numerical calculations.

The purpose of this section is to extend this analysis by deriving resummed expressions for the matching corrections to both the quartic coupling and the mass, incorporating simultaneously the contributions from all orders. This is achieved by exploiting the structure of the diagrammatic expansion and by applying standard resummation techniques to infinite classes of diagrams that share a fixed topology and differ only in the number of internal loops. (For a general introduction to perturbative expansions and summation methods, see Ref. [35], Chapter 23.)

We begin by focusing on a specific four external legs topology, which provides the most natural starting point for an all-order generalization of the matching corrections to the effective quartic coupling. Using the diagrammatic rules introduced in Ref. [31], the contribution of this diagram at generic order $\mathcal{O}(V^n)$ can be written as

$$D^{(n)} \doteq \begin{array}{c} \text{Diagram} \end{array} = \frac{1}{2} \left(\frac{\lambda}{4\pi R} \right)^n \sum_{1 \dots 2(n+1)} \delta_{12,34} \langle f | \phi_4^- \phi_3^- \phi_2^+ \phi_1^+ | i \rangle \times \frac{\prod_{j=0}^{n-2} \delta_{34,(5+2j)(6+2j)}}{\left(\prod_{j=5}^{2(n+1)} 2\omega_j \right) \left(\prod_{j=0}^{n-2} (\omega_3 + \omega_4 - \omega_{5+2j} - \omega_{6+2j}) \right)}. \quad (13)$$

Here we have introduced a shorthand notation for the momenta, $k_i = i$, and for the Kronecker delta, $\delta_{k_1+k_2=k_3+k_4} = \delta_{12,34}$. In the effective theory, the same diagram is evaluated under the constraint that all intermediate states have energies below the cut-off E_{\max} . At order $\mathcal{O}(V^n)$, the result is therefore multiplied by a product of Heaviside step functions which enforce these energy restrictions:

$$D^{(n)}|_{\text{eff}} \propto \prod_{j=1}^{n-1} \Theta(E_{\max} - \mathcal{E}_f + \omega_3 + \omega_4 - \omega_{2j+3} - \omega_{2j+4}). \quad (14)$$

Following Ref. [31], we simplify the non-trivial dependence on the external energies by working in the local approximation. Since we are interested in low-energy initial and final states, $\mathcal{E}_{i,f} \ll E_{\max}$, the dependence on external energies and momenta can be systematically expanded. Retaining only the leading term in this expansion amounts to evaluating the diagram at vanishing external energies and momenta. Within this approximation, the contribution of the diagram reduces to

$$D^{(n)} \simeq - \left(-\frac{\lambda}{4\pi R} \right)^n \pi R \int dx \langle f | [\phi^-]^2 [\phi^+]^2 | i \rangle \sum_{k_1, k_2, \dots, k_{n-1}} \frac{1}{\prod_{j=1}^{n-1} (2\omega_{k_j})^3}. \quad (15)$$

It is convenient to introduce the number of internal loops as an index, defined as $L \doteq n-1$. In the local approximation, the L -loop contribution factorizes into L identical momentum sums, so that the all-order sum reduces to a geometric series:

$$\begin{aligned} \sum_{L=1}^{\infty} D^{(L+1)} &\simeq -\pi R \int dx \langle f | [\phi^-]^2 [\phi^+]^2 | i \rangle \sum_{L=1}^{\infty} \left(-\frac{\lambda}{4\pi R} \right)^{L+1} \sum_{k_1, \dots, k_L} \prod_{j=1}^L \frac{1}{(2\omega_{k_j})^3} \\ &= \frac{\lambda}{4} \int dx \langle f | [\phi^-]^2 [\phi^+]^2 | i \rangle \sum_{L=1}^{\infty} \left(-\frac{\lambda}{4\pi R} \sum_k \frac{1}{(2\omega_k)^3} \right)^L \\ &= \frac{\lambda}{4} \int dx \langle f | [\phi^-]^2 [\phi^+]^2 | i \rangle \frac{X}{1-X}, \end{aligned} \quad (16)$$

where we defined

$$X \doteq -\frac{\lambda}{4\pi R} \sum_k \frac{1}{(2\omega_k)^3}. \quad (17)$$

The effective-theory result is obtained analogously, with the only modification coming from the cut-off constraint in Eq. (14), which amounts to replacing X by

$$X^{(\text{eff})} \doteq -\frac{\lambda}{4\pi R} \sum_k \frac{\Theta(E_{\max} - 2\omega_k)}{(2\omega_k)^3}. \quad (18)$$

Combining the full and effective expressions, we obtain

$$\sum_{L=1}^{\infty} D^{(L+1)} - \sum_{L=1}^{\infty} D^{(L+1)}|_{\text{eff}} \simeq \frac{\lambda}{4} \int dx \langle f | [\phi^-]^2 [\phi^+]^2 | i \rangle \left[\frac{X - X^{(\text{eff})}}{(1-X)(1-X^{(\text{eff})})} \right]. \quad (19)$$

This immediately yields the following result for the resummed matching correction to the quartic coupling

$$\delta\tilde{\lambda} = 6\lambda \left[\frac{X - X^{(\text{eff})}}{(1-X)(1-X^{(\text{eff})})} \right]. \quad (20)$$

We now turn to a two external legs topology, which yields the local matching correction associated to the mass. Generalizing this diagram to order $\mathcal{O}(V^n)$, one finds

$$B^{(n)} \doteq 2 \text{---} \begin{array}{c} 2n \\ \text{---} \end{array} \dots \begin{array}{c} 4 \\ \text{---} \end{array} \begin{array}{c} 6 \\ \text{---} \end{array} \text{---} 1 = \frac{\lambda}{18\pi R} \left(\frac{3\lambda}{4\pi R} \right)^{n-1} \sum_{1 \dots 2n+1} \delta_{1,2} \langle f | \phi_2^- \phi_1^+ | i \rangle \\ \times \frac{1}{2\omega_3} \prod_{j=1}^{n-1} \frac{\delta_{1,(2+2j)(3+2j)(3)}}{2\omega_{2+2j} 2\omega_{3+2j} (\omega_2 - \omega_3 - \omega_{2+2j} - \omega_{3+2j})}. \quad (21)$$

As before, in the effective theory the restriction to intermediate states with total energy below the cut-off is implemented through a product of step functions multiplying the entire expression, i.e.,

$$B^{(n)}|_{\text{eff}} \propto \prod_{j=1}^{n-1} \Theta(E_{\max} - \mathcal{E}_f + \omega_2 - \omega_3 - \omega_{2+2j} - \omega_{3+2j}). \quad (22)$$

Working again in the local approximation, the all-order sum takes the form

$$\begin{aligned} \sum_{L=1}^{\infty} B^{(L+1)} &\simeq \frac{\lambda}{18\pi R} \int dx \langle f | \phi^- \phi^+ | i \rangle \sum_{L=1}^{\infty} \left(\frac{3\lambda}{4\pi R} \right)^L \sum_k \frac{1}{2\omega_k} (G_k)^L \\ &= \frac{\lambda}{18\pi R} \int dx \langle f | \phi^- \phi^+ | i \rangle \sum_k \frac{1}{2\omega_k} \frac{NG_k}{1-NG_k}, \end{aligned} \quad (23)$$

where we defined

$$N \doteq \frac{3\lambda}{4\pi R} \quad \text{and} \quad G_k \doteq -\sum_j \frac{1}{2\omega_j 2\omega_{k+j} (\omega_k + \omega_j + \omega_{k+j})}. \quad (24)$$

The effective-theory result is obtained by enforcing the cut-off constraint from Eq. (22) directly in the loop sum, namely by replacing $G_k \rightarrow G_k^{(\text{eff})}$ with

$$G_k^{(\text{eff})} \doteq -\sum_j \frac{\Theta(E_{\max} - \omega_k - \omega_j - \omega_{k+j})}{2\omega_j 2\omega_{k+j} (\omega_k + \omega_j + \omega_{k+j})}. \quad (25)$$

Combining the contributions of the fundamental and effective theories, one obtains

$$\sum_{L=1}^{\infty} B^{(L+1)} - \sum_{L=1}^{\infty} B^{(L+1)}|_{\text{eff}} = \frac{\lambda}{18\pi R} \int dx \langle f | \phi^- \phi^+ | i \rangle \sum_k \frac{N}{2\omega_k} \left[\frac{G_k}{1-NG_k} - \frac{G_k^{(\text{eff})}}{1-NG_k^{(\text{eff})}} \right]. \quad (26)$$

This yields the resummed matching correction to the mass parameter,

$$\delta\tilde{m}^2 = \frac{\lambda}{9\pi R} \sum_k \frac{N}{2\omega_k} \left[\frac{G_k}{1 - NG_k} - \frac{G_k^{(\text{eff})}}{1 - NG_k^{(\text{eff})}} \right]. \quad (27)$$

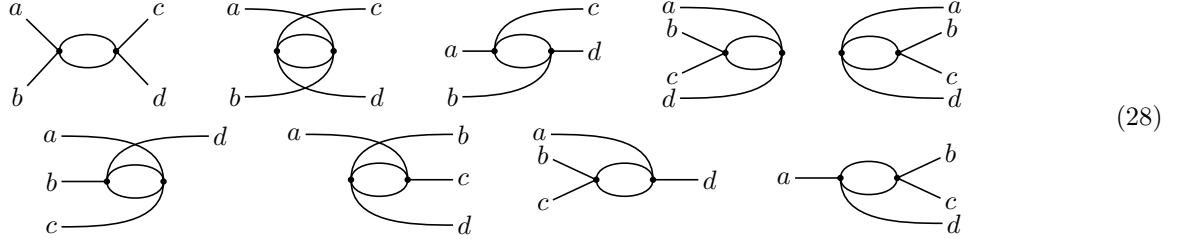
In conclusion, the resummed matching corrections to the quartic coupling and to the mass, given in Eqs. (20) and (27), respectively, provide compact all-order expressions that capture the dominant high-energy effects and will be implemented numerically in Sec. V to assess their quantitative impact on Hamiltonian-truncation results.

IV. NEXT-TO-NEXT-TO-LOCAL CORRECTIONS

Building on the framework of Ref. [32], sub-leading corrections arising from the effective matching procedure can be systematically derived. In particular, non-local contributions at order $\mathcal{O}(V^2)$ were shown to scale as $\mathcal{O}(E_{\max}^{-3})$, providing a further improvement over the leading local corrections, which already enhance the convergence of the bare HT. The resulting framework naturally organizes the corrections into a systematic expansion in inverse powers of the truncation scale E_{\max} .

At order $\mathcal{O}(V^3)$, local corrections scale as $\mathcal{O}(E_{\max}^{-4})$, while non-local contributions are suppressed by an additional power of E_{\max} , scaling as $\mathcal{O}(E_{\max}^{-5})$. Therefore, at order $\mathcal{O}(E_{\max}^{-4})$ one must include sub-leading components of the $\mathcal{O}(V^2)$ non-local corrections along with genuine $\mathcal{O}(V^3)$ local effects. In what follows, we extend the calculation of non-local contributions to $\mathcal{O}(E_{\max}^{-4})$ (hereafter referred to as the NNLO corrections) and provide a formulation that consistently incorporates the distributional nature of the matching coefficients.

We begin by classifying all diagrams with four external legs into nine distinct topologies, which differ in the construction of the intermediate state:



To extract the NNLO corrections, it is necessary to account for all possible symmetrizations of these diagrams, which are understood as inequivalent assignments of momentum indices for the intermediate states.

For simplicity, we focus on a single case with a four-leg external state, which admits only one topology. In this case, one must consider all six inequivalent pairs (b, c) , defined as

$$(b, c) \in \mathcal{C} \doteq \{(1, 2), (1, 3), (1, 4), (2, 3), (2, 4), (3, 4)\}. \quad (29)$$

Following the diagrammatic rules of Ref. [31], we obtain

$$\begin{aligned} \text{Diagram with four legs } a, b, c, d - \left[\text{Diagram with four legs } a, b, c, d \right]_{\text{eff}} &= \frac{1}{8} \left(\frac{\lambda}{2\pi R} \right)^2 \frac{1}{\dim(\mathcal{C})} \sum_{\substack{a, d, 5, 6 \\ (b, c) \in \mathcal{C}}} \delta_{abcd, 0} \delta_{bc, 56} \langle f | \phi_d^{(-)} \phi_c^{(-)} \phi_b^{(-)} \phi_a^{(-)} | i \rangle \\ &\quad \times \frac{\Theta(\mathcal{E}_f - \omega_b - \omega_c + \omega_5 + \omega_6 - E_{\max})}{2\omega_5 2\omega_6 (\omega_b + \omega_c - \omega_5 - \omega_6)}, \end{aligned} \quad (30)$$

where $a, d \in \{1, 2, 3, 4\}$, and with all indices mutually distinct, i.e., $a \neq b \neq c \neq d$. For other topologies, one obtains expressions that have similar structure to Eq. (30). The results can be systematically expanded by treating the IR scales $\omega_{a, b, c, d}$ and the external energies $\mathcal{E}_{f, i}$ as small compared to the UV scale set by the cut-off. Moreover, the momentum-conservation constraint $\delta_{bc, 56}$ enforces $\omega_5 \simeq \omega_6 \doteq \omega_k \simeq E_{\max}$.

This expansion is exactly the expansion of the non-local expression into a series of local terms. The first term of the series represent the purely local limit of the corrections, and the k -th term produces the next-to- k leading order (N^k LO) correction to the local term. The leading order (LO) and next-to-leading order (NLO) contributions have been already computed in the literature [31, 32], and we will focus on the NNLO contributions. At this order, the non-local factor appearing in the second line of Eq. (30) can be rewritten in terms of a universal symmetrized kernel

for the four-leg sector. Specifically, once all four-leg topologies in Eq. (28) and their inequivalent symmetrizations are included consistently, the result becomes independent of the particular external-leg assignment and can be expressed as

$$\begin{aligned} \mathcal{K}_{\text{sym}}^4(E_f, E_i, \Omega_4, \omega_k; E_{\max}) = & -\frac{2\Omega_4 + (E_f - E_i)^2 + 6\omega_k(E_f - E_i) + 24\omega_k^2}{32\omega_k^5} \Theta(2\omega_k - E_{\max}) \\ & -\frac{-2\Omega_4 - (E_f - E_i)^2 + 6\omega_k(E_f + E_i) + 3E_f(E_f - E_i)}{16\omega_k^4} \Theta'(2\omega_k - E_{\max}) \\ & -\frac{2\Omega_4 + (E_f - E_i)^2 + 6E_f E_i}{16\omega_k^3} \Theta''(2\omega_k - E_{\max}), \end{aligned} \quad (31)$$

where $\Theta'(2\omega_k - E_{\max})$, $\Theta''(2\omega_k - E_{\max})$ are, respectively, the first and second derivatives of the Heaviside distribution, and $\Omega_4 \doteq \omega_1^2 + \omega_2^2 + \omega_3^2 + \omega_4^2$. We emphasize that the kernel $\mathcal{K}_{\text{sym}}^4$ exhibits a clear hierarchy in its dependence on the external energies. At LO it is completely independent of E_i and E_f . At NLO it depends on the total energies of the initial and final states, but not on the individual external frequencies. At NNLO it acquires an irreducible dependence on the external frequencies, which enters only through the quadratic combination Ω_4 .

To make the operator content explicit, consider the general expansion of Eq. (31) at order n . Once all four-leg topologies are accounted for, one generically encounters monomials $E_f^m E_i^l$ with $m + l \leq n$, which translate into the operators

$$E_f^m E_i^l \longrightarrow H_0^m : \phi^4 : H_0^l. \quad (32)$$

In addition, the Ω_4 -dependence forces the inclusion of further operator structures. Considering again, as an explicit example, the topology in Eq. (30), one finds

$$\begin{aligned} & \sum_{1,2,3,4} \delta_{12,34}(\omega_1^2 + \omega_2^2 + \omega_3^2 + \omega_4^2) \langle f | \phi_4^- \phi_3^- \phi_2^- \phi_1^- | i \rangle \\ & = \frac{1}{2\pi R} \sum_{k_1, k_2, k_3, k_4} \delta_{k_1 k_2, k_3 k_4} \frac{\omega_{k_1}^2 + \omega_{k_2}^2 + \omega_{k_3}^2 + \omega_{k_4}^2}{\sqrt{2\omega_{k_1}} \sqrt{2\omega_{k_2}} \sqrt{2\omega_{k_3}} \sqrt{2\omega_{k_4}}} \langle f | a_{k_4}^\dagger a_{k_3}^\dagger a_{k_2}^\dagger a_{k_1}^\dagger | i \rangle. \end{aligned} \quad (33)$$

All these operators must therefore be incorporated into the effective Hamiltonian as independent operator contributions, each multiplied by the corresponding numerical coefficients determined by the matching procedure.

Factors of ω_p multiplying the fields admit a natural interpretation in the interaction picture. Indeed, the mode operators obey

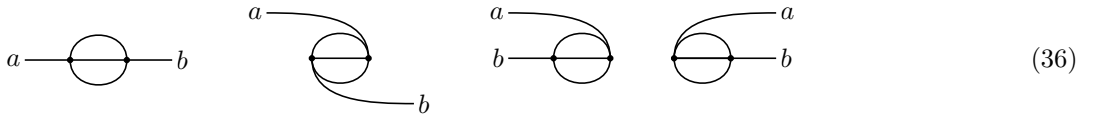
$$\partial_t \phi_p^\pm = \mp i \omega_p \phi_p^\pm = i[H_0, \phi_p^\pm], \quad (34)$$

so that insertions of a single power of the frequency can be equivalently represented either as time derivatives acting on the fields or as commutators with the free Hamiltonian. Since the dependence on the external frequencies enters the kernel $\mathcal{K}_{\text{sym}}^4$ only through the combination Ω_4 , in which all frequencies appear quadratically, it is naturally associated with second-order time derivatives, or equivalently with double commutators with H_0 . Indeed, one finds

$$\omega_p^2 \phi_p^\pm = -\partial_t^2 \phi_p^\pm = [H_0, [H_0, \phi_p^\pm]], \quad (35)$$

independently of the sign of the frequency. This structure reflects the emergence of higher-derivative operator contributions at NNLO.

Diagrams with two external legs can be treated in complete analogy. They are classified into the following four topologies



The resulting expressions mirror those of the four-leg case in Eq. (31). After summing over all topologies in Eq. (36) and performing the corresponding symmetrizations, the NNLO non-local corrections can be organized in terms of a universal symmetrized kernel $\mathcal{K}_{\text{sym}}^2$, whose structure is independent of the specific external-leg assignment. The associated operatorial content follows from the mapping of energy factors according to

$$E_f^m E_i^l \longrightarrow H_0^m : \phi^2 : H_0^l. \quad (37)$$

At NNLO, the two-leg sector develops the same non-local feature as in the four-leg case, namely the appearance of additional contributions proportional to $\Omega_2 \doteq \omega_1^2 + \omega_2^2$. Again, this encodes an irreducible dependence on the individual external frequencies, which enter the kernel $\mathcal{K}_{\text{sym}}^2$ exclusively through a quadratic combination, in direct analogy with the role played by Ω_4 .

The case with no external legs is simpler, as only the following topology contributes


(38)

The corresponding operatorial contributions involve only powers of the free Hamiltonian, according to

$$E_i^{m+l} = E_f^{m+l} \longrightarrow \langle f | H_0^{m+l} | i \rangle, \quad (39)$$

In order to determine the numerical coefficients multiplying the various operatorial structures discussed above, one must examine the distributional contributions arising in the expansion of the matching expressions. At order n in this expansion, terms proportional to the n -th derivative of the Heaviside step function typically appear. Considering the four-external-leg case in Eq. (31), these contributions schematically take the form

$$\sum_k \frac{1}{\omega_k^\alpha} \frac{d^n}{d(2\omega_k)^n} \Theta(2\omega_k - E_{\max}). \quad (40)$$

In finite volume the spectrum is discrete, therefore distributions such as $\delta(2\omega_k - E_{\max})$ (and higher derivatives of Θ as well) do not correspond to a unique numerical prescription: if one tries, e.g., to assign the prescription

$$\delta(2\omega_k - E_{\max}) = \begin{cases} 1 & \text{if } 2\omega_k = E_{\max} \\ 0 & \text{otherwise} \end{cases}, \quad (41)$$

the resulting contribution vanishes for generic values of E_{\max} , R , and m , since the condition $2\omega_k = E_{\max}$ requires

$$k = R \sqrt{\frac{E_{\max}^2}{4} - m^2} \quad (42)$$

to be an integer, which is not guaranteed for generic choices of the parameters.

This issue is not intrinsic to the matching procedure, but rather an artifact of performing the $1/E_{\max}$ expansion after the spectrum discretization. Formulating the matching in infinite volume provides a natural way to avoid it, as the spectrum becomes continuous and the distributional structure associated with derivatives of the Heaviside step function is well defined in the standard sense. Once the coefficients are determined in the continuum, the discretization can be reintroduced through spatial compactification, which is required in practice to obtain a separable Hilbert space.

In infinite volume, the sum in Eq. (40) is replaced by a momentum integral, leading to

$$F_n^\alpha(E_{\max}) \doteq \int_{-\infty}^{\infty} dk \frac{1}{\omega(k)^\alpha} \frac{d^n}{d(2\omega(k))^n} \Theta(2\omega(k) - E_{\max}). \quad (43)$$

The discussion above can be straightforwardly extended to the cases with two and zero external legs. In these sectors, the determination of the matching coefficients similarly reduces to the evaluation of continuum integrals involving derivatives of the Heaviside step function, with the only difference being the structure of the energy denominators associated with the corresponding topologies. In the two-leg case, the relevant integrals take the form

$$I_n^\alpha(E_{\max}) \doteq \int_{-\infty}^{\infty} dk \int_{-\infty}^{\infty} dq \frac{1}{P_2(k, q) W_2^\alpha(k, q)} \frac{d^n}{dW_2(k, q)^n} \Theta(W_2(k, q) - E_{\max}), \quad (44)$$

where we have defined

$$P_2(k, q) \doteq \omega(k) \omega(q) \omega(k + q), \quad W_2(k, q) \doteq \omega(k) + \omega(q) + \omega(k + q). \quad (45)$$

Similarly, diagrams with no external legs give rise to

$$B_n^\alpha(E_{\max}) \doteq \int_{-\infty}^{\infty} dk \int_{-\infty}^{\infty} dp \int_{-\infty}^{\infty} dq \frac{1}{P_0(k, p, q) W_0^\alpha(k, p, q)} \frac{d^n}{dW_0(k, p, q)^n} \Theta(W_0(k, p, q) - E_{\max}), \quad (46)$$

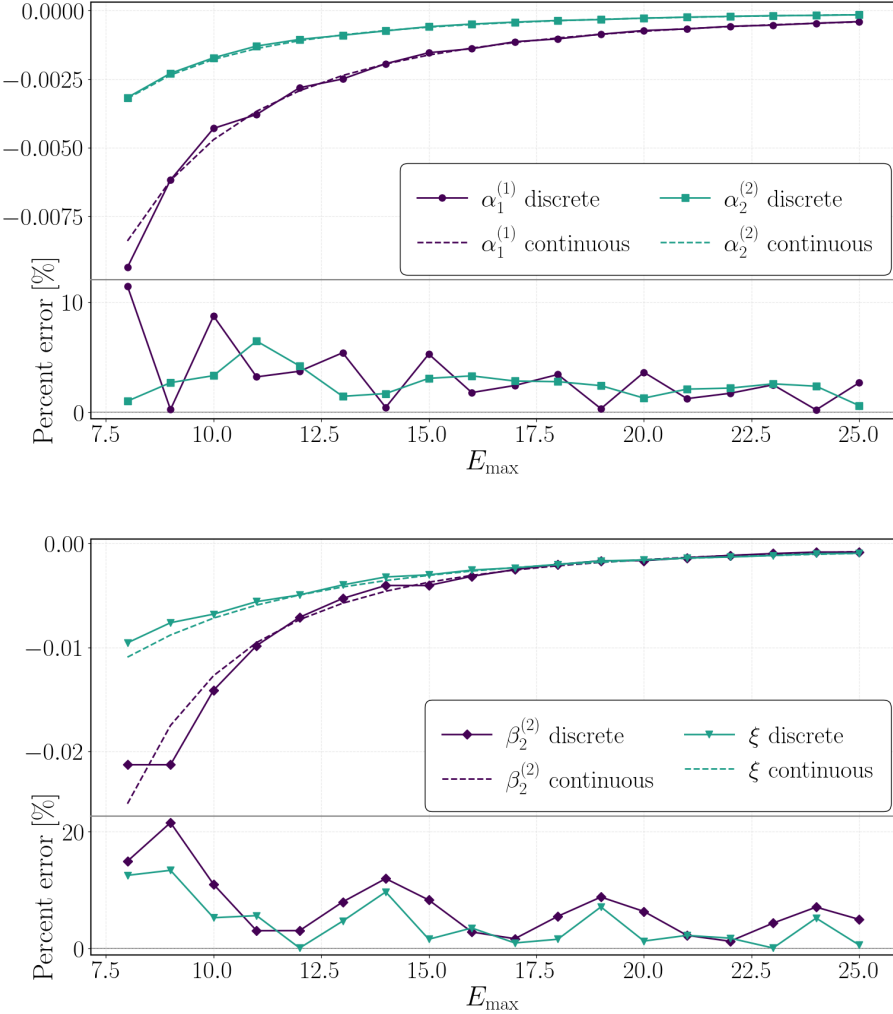


FIG. 1. First non-local corrections ξ , $\alpha_1^{(2)}$, $\alpha_2^{(2)}$, and $\beta_2^{(2)}$, computed at finite (continuous line) and infinite (dotted line) volume as a function of the energy cut-off E_{\max} , for $2\pi R = 10$, $\lambda/4\pi = 1$ and $m = 1$, in the range $E_{\max} \in [8, 25]$. The upper panel shows the corrections $\alpha_1^{(2)}$ and $\alpha_2^{(2)}$, while the lower panel shows ξ and $\beta_2^{(2)}$. In both panels, the lower portion of each plot shows the corresponding percent error with respect to the continuum value. For the discrete corrections, the sums over momenta are evaluated up to a finite maximum momentum $K_{\text{UV}} = 1000$.

with

$$P_0(k, p, q) \doteq \omega(k) \omega(p) \omega(q) \omega(k + p + q), \quad W_0(k, p, q) \doteq \omega(k) + \omega(p) + \omega(q) + \omega(k + p + q). \quad (47)$$

The explicit evaluation of the integrals F_n^α , I_n^α , and B_n^α is technically non-trivial, due to the presence of derivatives of the Heaviside step function and the non-linear dependence of the integrands on the integration variables. The calculation is therefore deferred to App. A, where we describe the general strategy and provide the details of the derivation.

In Ref. [32], the first non-local coefficients, $\xi, \alpha_1^{(1)}, \alpha_2^{(2)}, \beta_1^{(1)}, \beta_2^{(2)}$, are derived; the corresponding expressions are reported in App. B for completeness.

Their determination relies on different practical prescriptions. Some coefficients are computed directly in infinite volume, for example $\beta_1^{(1)}$, while others are evaluated as discrete sums over finite-volume modes, such as $\beta_2^{(2)}$.

These definitions coincide in the infinite-volume limit. However, at the finite volumes relevant for numerical implementations, they can yield quantitatively different results, as discussed in App. C. To have a single and consistent definition for all coefficients, we adopt an infinite-volume matching.

Figure 1 shows the ratio between the leading non-local corrections computed at finite and infinite volume as a

function of the energy cut-off E_{\max} . At low E_{\max} , the discrete evaluation fluctuates around the continuum result, indicating the presence of finite-volume effects. For larger values of E_{\max} , the discrete results instead converge to the continuum corrections, which exhibit a smooth and stable behavior as E_{\max} is varied.

Having determined the matching coefficients in infinite volume, we can now address the problem of implementing the resulting operatorial structures in a separable Hilbert space. This requires compactifying the spatial direction, which discretizes the spectrum and makes it possible to evaluate the operators on a finite truncated basis. The compact spatial geometry is therefore introduced only at this stage, as the matching calculation itself does not require a discrete spectrum.

The effective Hamiltonian thus contains contributions that combine continuum matching coefficients with operators defined in finite volume. Table I summarizes the results, presenting each operator together with its corresponding correction, where we have introduced the operators H_2 and H_4 as

$$H_2 \doteq \int R d\theta : \phi^2 : , \quad H_4 \doteq \int R d\theta : \phi^4 : . \quad (48)$$

The operators and their associated corrections are organized according to their scaling in inverse powers of the truncation scale E_{\max} , from which we can confirm that the second non-local corrections scale as $\mathcal{O}(E_{\max}^{-4})$.

Lower orders		Higher order	
Operator	Coefficient	Operator	Coefficient
$\mathcal{O}(E_{\max}^{-2})$		$\mathcal{O}(E_{\max}^{-4})$	
I	$-\frac{\lambda^2 R}{1536\pi^2} B_0^1$	H_0^2	$-\frac{\lambda^2 R}{768(2\pi)^2} B_2^1$
H_2	$-\frac{\lambda^2}{96\pi^2} I_0^1$	$H_0^2 H_2$	$-\frac{\lambda^2}{192\pi^2} I_1^2$
H_4	$-\frac{3\lambda^2}{16\pi} F_0^3$	$H_0^2 H_4$	$-\frac{\lambda^2}{128\pi} (F_0^5 + 4F_1^4 + 2F_2^3)$
$\mathcal{O}(E_{\max}^{-3})$		$H_4 H_0^2$	$-\frac{\lambda^2}{128\pi} (F_0^5 - 2F_1^4 + 2F_2^3)$
H_0	$-\frac{\lambda^2 R}{384(2\pi)^2} B_1^1$	$H_0 H_2 H_0$	$-\frac{\lambda^2}{192\pi^2} (-I_1^2 + I_2^1)$
$H_0 H_2$	$-\frac{\lambda^2}{192\pi^2} (I_0^2 + I_1^1)$	$H_0 H_4 H_0$	$-\frac{\lambda^2}{64\pi} (-F_0^5 - F_1^4 + 4F_2^3)$
$H_0 H_4$	$-\frac{3\lambda^2}{64\pi} (F_0^4 + 2F_1^3)$	$\sim \Omega_2 H_2$	$-\frac{\lambda^2}{384\pi^2} (2I_0^3 - 2I_1^2 + I_2^1)$
$H_2 H_0$	$-\frac{\lambda^2}{192\pi^2} (-I_0^2 + I_1^1)$	$\sim \Omega_4 H_4$	$-\frac{\lambda^2}{64\pi} (F_0^5 - 2F_1^4 + 2F_2^3)$
$H_4 H_0$	$-\frac{3\lambda^2}{64\pi} (-F_0^4 + 2F_1^3)$		

TABLE I. Operators organized according to their scaling in inverse powers of the truncation scale E_{\max} . Lower-order contributions are shown in the left column, while the $\mathcal{O}(E_{\max}^{-4})$ terms associated with the second non-local corrections are collected in the right column. When entering the effective Hamiltonian, the contributions involving H_4 and H_2 must be divided by the appropriate symmetry factors, namely 4! and 2, respectively.

In the zero-external-leg sector, the NNLO operatorial structure involves only powers of the free Hamiltonian H_0 , see Eq. (39). Moreover, the coefficients arising from derivatives of the Heaviside distribution can always be rewritten as derivatives with respect to the cut-off (see Eq. (A1) in App. A). At order n , the corresponding numerical prefactor scales as $1/n!$. As a result, the full tower of non-local contributions in the vacuum sector can be resummed into a compact operator, i.e.,

$$\sum_{n=0}^{\infty} \frac{1}{n!} H_0^n (-\partial_{E_{\max}})^n B_0^1(E_{\max}) = e^{-H_0 \partial_{E_{\max}}} B_0^1(E_{\max}) = B_0^1(E_{\max} - H_0), \quad (49)$$

where the last equality is defined through the Taylor expansion of $B_0^1(E_{\max} - H_0)$. Equivalently, when acting on an eigenstate of H_0 with energy \mathcal{E} , it yields $B_0^1(E_{\max} - \mathcal{E})$. This shows that, in the vacuum sector, the non-local $1/E_{\max}$ expansion resums exactly to an operator-valued function of H_0 .

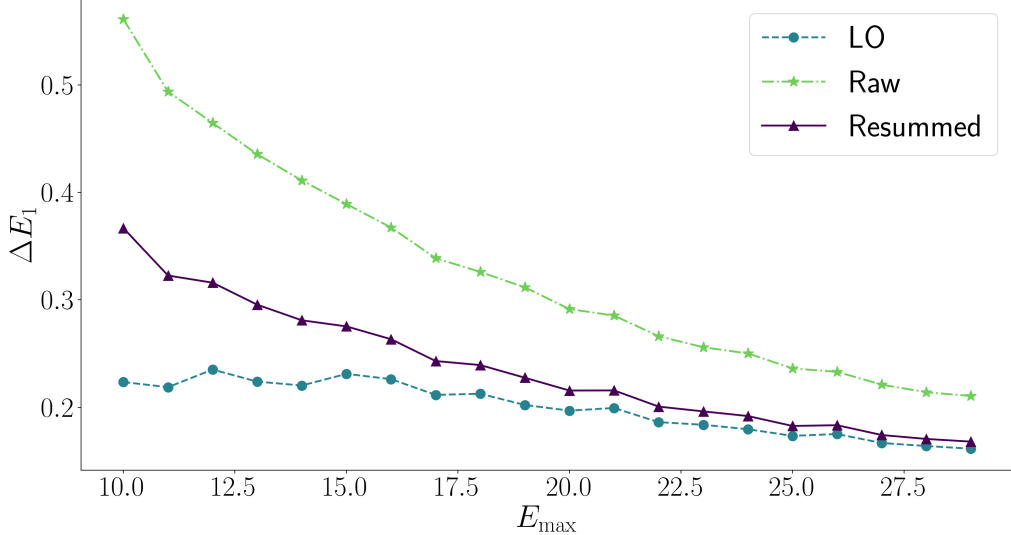


FIG. 2. First energy gap ΔE_1 as a function of the truncation scale E_{\max} , at fixed parameters $m = 1$, $\lambda/(4\pi) = 1$, and $2\pi R = 10$. The curve (dot-dashed lines with star markers) labeled “Raw” corresponds to the bare truncation $H_{\text{raw}} = PHP$. The curve (dashed lines with circular markers) labeled “LO” includes the leading local counterterms. The curve (solid lines with triangular markers) labeled “Resummed” includes the resummed local corrections implemented via Eqs. (20) and (27).

V. NUMERICAL RESULTS

In this section we implement the resummed matching corrections to the quartic coupling and to the quadratic operator, given in Eqs. (20) and (27) and derived in Sec. III, together with the NNLO non-local operator insertions summarized in Tab. I and discussed in Sec. IV.

For each value of the truncation scale E_{\max} we construct the truncated Hilbert space \mathcal{H}_{tru} and diagonalize the corresponding Hamiltonian matrix. The database containing all eigenvalues extracted from the effective Hamiltonians, for the various prescriptions employed in the analysis of this section, can be found in Ref. [36].

As a representative observable we consider the first spectral gap,

$$\Delta E_1(E_{\max}) \doteq E_1(E_{\max}) - E_0(E_{\max}), \quad (50)$$

where E_0 and E_1 denote the lowest two eigenvalues of the effective Hamiltonian.

Figure 2 compares ΔE_1 obtained from three prescriptions: (i) the raw truncation $H_{\text{raw}} \doteq PHP$; (ii) the LO improvement, where only the lowest-order local counterterms are included; (iii) the resummed local improvement, where the local counterterms are implemented using the all-order expressions for $\delta\tilde{\lambda}(E_{\max})$ and $\delta\tilde{m}^2(E_{\max})$ from Sec. III.

In the range of E_{\max} explored here, the “resummed” prescription does not exhibit a systematic improvement over the LO result. The underlying reason is that the resummation does not provide a uniformly improved approximation order by order: it resums to all orders only a fixed diagrammatic topology and only within the local approximation. In this regime, non-local contributions can be numerically comparable to the higher-order local terms that are being resummed, and additional diagrammatic topologies may yield significant contributions at the same order in the $1/E_{\max}$ expansion.

Resumming only the local contributions can lead to over-correction, which may slow the convergence with E_{\max} . In contrast, the LO-improved Hamiltonian includes all local corrections at $O(V^2)$ through a controlled perturbative matching, ensuring more reliable convergence.

This observation motivates the inclusion of the non-local operator insertions discussed in Sec. IV and summarized in Tab. I, which account for the missing sub-leading contributions in the $1/E_{\max}$ expansion.

Before addressing the NNLO corrections, Fig. 3 compares the first energy gap ΔE_1 obtained from discrete (finite-volume) and continuous (infinite-volume) evaluations for two values of the circumference, $L = 10$ and $L = 15$, at LO and NLO.

Comparing the two orders shows that the discrepancy between the discrete and continuous treatments decreases as the cut-off E_{\max} is increased. Moreover, apart from isolated spikes, increasing the volume from $L = 10$ to $L = 15$

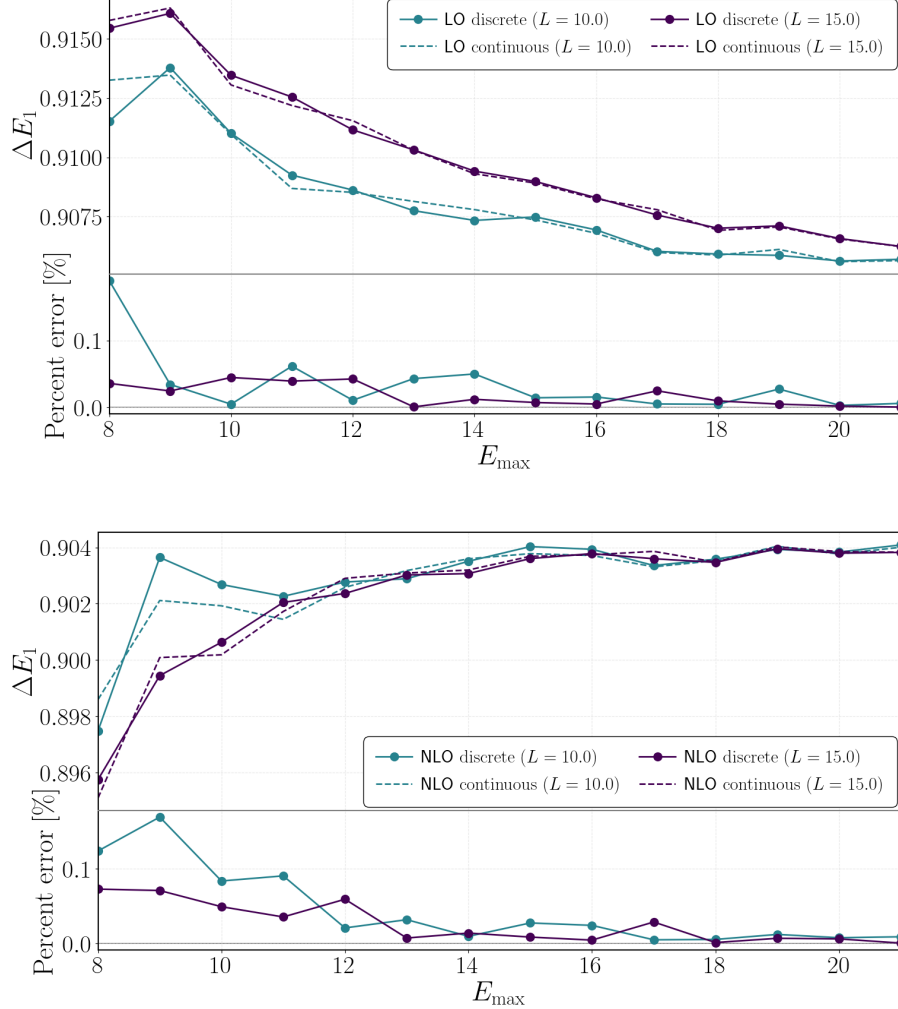


FIG. 3. First energy gap ΔE_1 as a function of the cut-off E_{\max} for two circumferences, $L = 10$ and $L = 15$, at fixed parameters $m = 1$ and $\lambda/(4\pi) = 1$. The upper panel shows the LO implementation (including corrections up to $\mathcal{O}(E_{\max}^{-2})$), while the lower panel shows the NLO implementation (including corrections up to $\mathcal{O}(E_{\max}^{-3})$). In each panel, the lower sub-plot reports the percent deviation of the discrete result from the corresponding continuous evaluation. We observe that, in the infinite-dimensional case, the dependence of the spectrum on the value of the circumference originates from the operatorial sector rather than from the coefficients.

systematically suppresses residual finite-volume effects and results in faster and more uniform convergence to the continuum limit as E_{\max} increases.

We conclude by presenting the numerical results for the NNLO non-local corrections summarized in Tab. I. Figure 4 shows the first energy gap ΔE_1 and the higher gap $\Delta E_5 \doteq E_5 - E_0$ as functions of E_{\max} , with ΔE_5 varying more smoothly with the cut-off. Both observables are displayed for two values of the coupling, $\lambda/(4\pi) = 1$ and $\lambda/(4\pi) = 3$. For each configuration, all truncation prescriptions are implemented, namely Raw, LO, NLO, and NNLO.

Across the four panels in Fig. 4, the main qualitative trend is that higher-order HTET corrections progressively reduce the residual E_{\max} -dependence of the extracted gaps. In particular, compared to the raw truncation and the LO prescriptions, both NLO and NNLO display a markedly flatter behavior as E_{\max} increases.

At low E_{\max} , the NNLO curves can display a stronger variation, in particular at larger coupling, where the NNLO points approach the asymptotic region from below with a pronounced rise. However, as E_{\max} increases, the NNLO results converge rapidly and become nearly indistinguishable from the NLO ones, reaching an approximately constant plateau already at intermediate cut-offs. In this sense, the NNLO prescription does not improve the behavior at the smallest truncations, but it ensures faster convergence toward the large- E_{\max} regime and a comparably stable plateau once E_{\max} is sufficiently large.

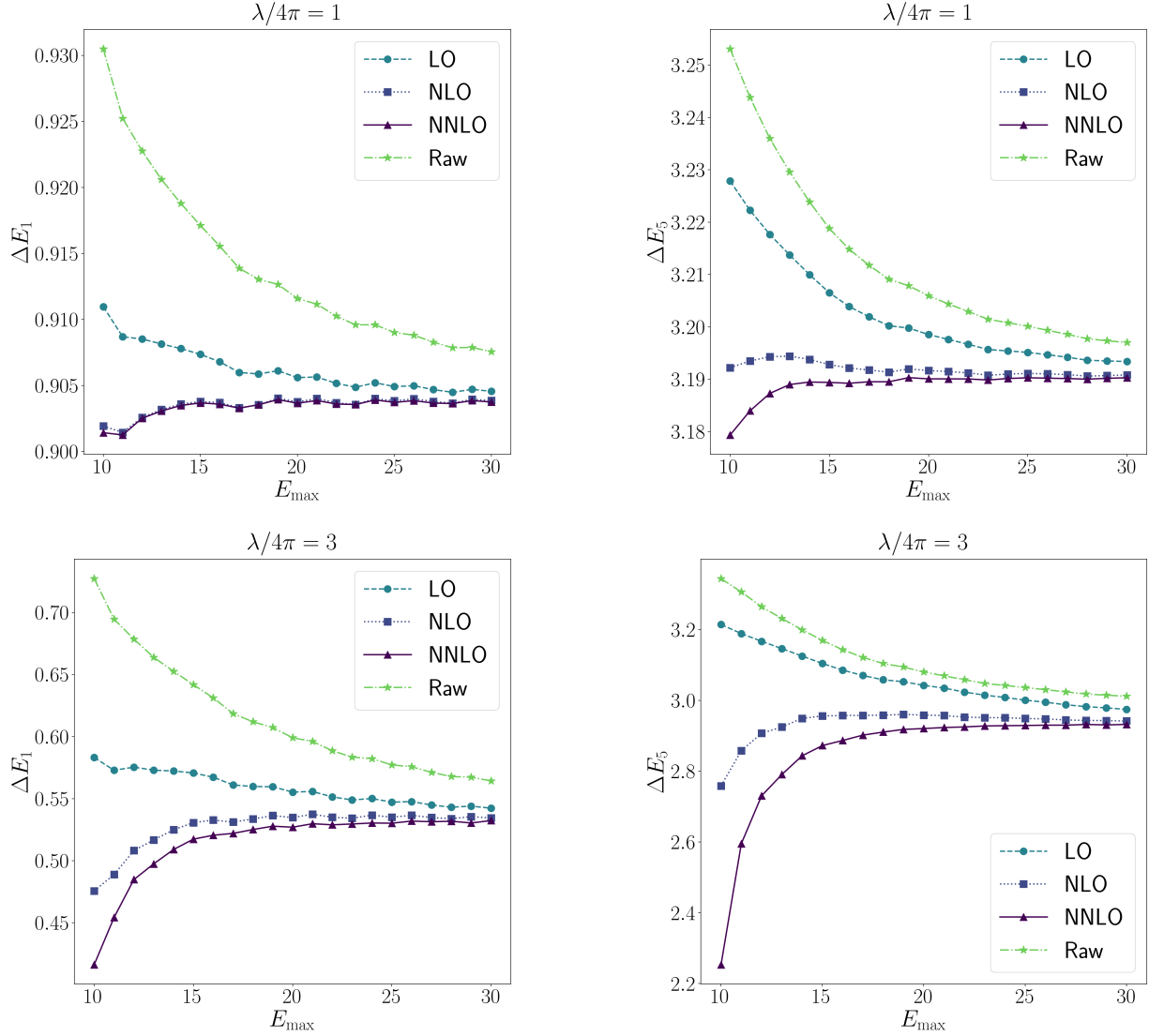


FIG. 4. Dependence of the energy gaps on the cut-off E_{\max} , comparing different HT and HTET prescriptions: Raw (stars with dash-dotted lines), LO (circles with dashed lines), NLO (squares with dotted lines), and NNLO (triangles with solid lines). Clockwise from the top left: ΔE_1 with $\lambda/(4\pi) = 1$, ΔE_5 with $\lambda/(4\pi) = 1$, ΔE_5 with $\lambda/(4\pi) = 3$, and ΔE_1 with $\lambda/(4\pi) = 3$.

VI. CONCLUSION

In this work we investigated HT for the two-dimensional $\lambda\phi^4$ theory within the HTET framework, where truncation effects are organized as a controlled expansion in inverse powers of the UV cut-off E_{\max} .

Building on the $\mathcal{O}(V^2)$ matching program of Ref. [31], we developed two complementary improvements.

First, we derived compact all-order expressions for the local matching corrections to the quartic coupling and the mass, obtained by resumming infinite classes of diagrams sharing a fixed topology within the local approximation.

Second, we extended the non-local sector beyond the leading terms by deriving the NNLO operator insertions contributing at $\mathcal{O}(E_{\max}^{-4})$, following and extending the systematic strategy of Ref. [32]. These contributions are particularly relevant because, in view of a systematic $\mathcal{O}(V^3)$ HTET program, they scale with the same power of $1/E_{\max}$ as the next local corrections.

On the numerical side, we quantified these improvements through the cut-off dependence of low-energy spectral gaps. The resummed local prescription, implemented through Eqs. (27) and (20), does not yield a uniform improvement over the LO result in the explored range of E_{\max} . This behavior is consistent with the fact that the resummation captures only a restricted subset of UV contributions, a fixed topology treated in the local approximation, while non-local terms and additional topologies entering at the same order in the $1/E_{\max}$ expansion can be numerically comparable to (or

larger than) the higher-order local terms being resummed. As a consequence, resumming this local subclass alone can lead to an overcorrection and to an apparently slower convergence with E_{\max} than the LO-improved Hamiltonian, which instead implements a controlled matching at fixed perturbative order and includes the complete $\mathcal{O}(V^2)$ local correction.

These observations motivated the inclusion of genuinely non-local operator insertions. A central technical point is that at NNLO the matching coefficients acquire distributional contributions involving derivatives of Heaviside step functions. At finite volume, where the spectrum is discrete, introducing such distributions after discretization leads to an ambiguous numerical prescription. We resolved this issue by determining the matching coefficients in infinite volume, where the distributional structure is unambiguously defined, and only then we moved to finite volume to implement the operators on a separable truncated Hilbert space, in the spirit of a continuum-first matching [32]. The resulting effective Hamiltonian combines continuum coefficients with finite-volume operators (summarized in Tab. I) and provides a systematic NNLO extension of the non-local sector.

Our numerical results showed a clear trend: higher-order HTET corrections progressively reduce the residual E_{\max} -dependence of the extracted gaps. Relative to the raw and LO truncation schemes, both NLO and NNLO results display a markedly flatter behavior as E_{\max} increases. At smaller cut-offs, NNLO results can vary more strongly, especially at larger coupling, but they rapidly approach the large- E_{\max} regime and become nearly indistinguishable from NLO results at intermediate truncations, while maintaining a stable plateau once E_{\max} is sufficiently large. For reproducibility, the spectra used to produce the figures are available in the accompanying database [36].

Overall, our analysis supports a consistent picture: a systematic HTET expansion beyond the leading local approximation is feasible, but its practical effectiveness depends on two closely related conditions. From the analytical side, one must expand all previously derived non-local structures to the desired order in $1/E_{\max}$, since sub-leading terms from lower-order non-local contributions can enter at the same parametric order as genuinely higher-order corrections. From the numerical side, one must implement an increasingly richer operator basis, including higher-derivative structures associated with the irreducible dependence on external frequencies, and efficiently evaluate the corresponding matrix elements on the truncated Hilbert space.

In conclusion, a systematic HTET expansion must address both aspects, with the broader goal of improving precision at moderate truncation scales and of generalizing these framework to other quantum field theories and higher-dimensional settings.

Appendix A: Integral computation

In this appendix we discuss the explicit evaluation of the integrals F_n^α , I_n^α , and B_n^α , which enter the determination of the matching coefficients. Their computation is technically non-trivial, due to the presence of derivatives of the Heaviside step function and to the non-linear dependence of its argument on the integration variables.

A first simplification follows from the observation that derivatives acting on the integration variables can be equivalently transferred to derivatives with respect to the energy cut-off. Considering F_n^α as an example, one finds

$$\frac{d^n}{d(2\omega(k))^n} \Theta(2\omega(k) - E_{\max}) = (-1)^n \frac{d^n}{dE_{\max}^n} \Theta(2\omega(k) - E_{\max}), \quad (\text{A1})$$

which immediately implies

$$F_n^\alpha(E_{\max}) = (-1)^n \frac{d^n}{dE_{\max}^n} F_0^\alpha(E_{\max}). \quad (\text{A2})$$

Therefore, it is sufficient to compute $F_0^\alpha(E_{\max})$ once and obtain all higher- n functions by differentiation with respect to E_{\max} . The same simplification applies to the integrals I_n^α and B_n^α , where the derivatives with respect to W_2 and W_4 can be similarly re-expressed as derivatives with respect to E_{\max} .

A further simplification follows from the observation that the integrals scale with the mass according to

$$\begin{aligned} I_n^\alpha(E_{\max}; m) &= m^{-\Delta_I} I_n^\alpha(E; 1), \quad \Delta_I = 1 + \alpha + n, \\ F_n^\alpha(E_{\max}; m) &= m^{-\Delta_F} F_n^\alpha(E; 1), \quad \Delta_F = \alpha + n - 1, \\ B_n^\alpha(E_{\max}; m) &= m^{-\Delta_B} B_n^\alpha(E; 1), \quad \Delta_B = 1 + \alpha + n, \end{aligned} \quad (\text{A3})$$

with $E \doteq E_{\max}/m$. Therefore, without loss of generality, we can compute the integrals for $m = 1$ and restore the mass dependence a posteriori. In the case with four external legs, it is sufficient to evaluate $F_0^\alpha(E, 1)$, whose numerical computation is straightforward.

The situation is more involved in the case with two external legs, where one has to determine $I_0^\alpha(E, 1)$. Here one can proceed by noting that both $P_2(k, q)$ and $W_2(k, q)$, which from now on we denote simply by $P(k, q)$ and $W(k, q)$, depend only on k^2 , q^2 , and $(k+q)^2$. This allows us to reduce the integral to

$$I_0^\alpha(E) = 2 \int_0^\infty dk \int_{-\infty}^\infty dq \frac{1}{P(k, q)W^\alpha(k, q)} \Theta(W(k, q) - E). \quad (\text{A4})$$

Now we can decompose $I_0^\alpha(E)$ into three distinct contributions:

$$\begin{aligned} I_0^\alpha(E) &= I_{0,U}^\alpha(E) + I_{0,L}^{<,\alpha}(E) + I_{0,L}^{>,\alpha}(E), \\ I_{0,U}^\alpha(E) &= 2 \int_0^\infty dk \int_0^\infty dq \frac{1}{P(k, q)W^\alpha(k, q)} \Theta(W(k, q) - E), \\ I_{0,L}^{<,\alpha}(E) &= 2 \int_0^\infty dk \int_0^{k/2} dq \frac{1}{P(k, -q)W^\alpha(k, -q)} \Theta(W(k, -q) - E), \\ I_{0,L}^{>,\alpha}(E) &= 2 \int_0^\infty dk \int_{k/2}^\infty dq \frac{1}{P(k, -q)W^\alpha(k, -q)} \Theta(W(k, -q) - E), \end{aligned} \quad (\text{A5})$$

where each individual integral is such that the function W is monotonic with respect to q at fixed k . We can therefore perform the change of integration variable $z = W(k, \pm q)$ at fixed k , obtaining:

$$I_{0,U}^\alpha(E) = 2 \int_0^\infty dk \int_{W(k,0)}^\infty \frac{dz}{z^\alpha} \frac{J(k, z)}{P(k, q_U(k, z))} \Theta(z - E), \quad (\text{A6})$$

$$I_{0,L}^{<,\alpha}(E) = 2 \int_0^\infty dk \int_{W(k,-k/2)}^{W(k,0)} \frac{dz}{z^\alpha} \frac{J(k, z)}{P(k, q_L^{<}(k, z))} \Theta(z - E), \quad (\text{A7})$$

$$I_{0,L}^{>,\alpha}(E) = 2 \int_0^\infty dk \int_{W(k,-k/2)}^\infty \frac{dz}{z^\alpha} \frac{J(k, z)}{P(k, q_L^{>}(k, z))} \Theta(z - E), \quad (\text{A8})$$

where we defined the inverse transformations as

$$q_U(k, z) = -\frac{k}{2} + \sqrt{\frac{k^2}{4} + \frac{R^2(k, z) - k^2 - 1}{2(1 + R(k, z))}} \quad \text{for } I_{0,U}^\alpha(E), \quad (\text{A9})$$

$$q_L^{<}(k, z) = \frac{k}{2} - \sqrt{\frac{k^2}{4} + \frac{R^2(k, z) - k^2 - 1}{2(1 + R(k, z))}} \quad \text{for } I_{0,L}^{<,\alpha}(E), \quad (\text{A10})$$

$$q_L^{>}(k, z) = \frac{k}{2} + \sqrt{\frac{k^2}{4} + \frac{R^2(k, z) - k^2 - 1}{2(1 + R(k, z))}} \quad \text{for } I_{0,L}^{>,\alpha}(E), \quad (\text{A11})$$

with

$$R(k, z) = \frac{z^2 - 1}{2} - z\omega(k), \quad J(k, z) = \frac{d}{dz} \left[\sqrt{\frac{k^2}{4} + \frac{R^2(k, z) - k^2 - 1}{2(1 + R(k, z))}} \right], \quad (\text{A12})$$

being $J(k, z)$ the Jacobian of the variable transformation.

Now we can use the theta-function $\Theta(z - E)$ explicitly to change the integration limits. In conclusion, we obtain

$$\begin{aligned} I_0^\alpha(E) &= 2 \int_0^\infty dk \int_{\max(E, W(k,0))}^\infty \frac{dz}{z^\alpha} \frac{J(k, z)}{P(k, q_U(k, z))} \\ &\quad + 2 \int_{k^*(E)}^\infty dk \int_{\max(E, W(k, -k/2))}^{W(k,0)} \frac{dz}{z^\alpha} \frac{J(k, z)}{P(k, q_L^{<}(k, z))} \\ &\quad + 2 \int_0^\infty dk \int_{\max(E, W(k, -k/2))}^\infty \frac{dz}{z^\alpha} \frac{J(k, z)}{P(k, q_L^{>}(k, z))}, \end{aligned} \quad (\text{A13})$$

where we defined

$$k^*(E) \doteq \sqrt{\frac{(E-1)^2}{4} - 1}, \quad (\text{A14})$$

which is the minimum value of k such that $W(k, 0) > E$.

Now, the integral in the form above can be easily computed for any value of E by means of a quadrature routine. To take derivatives, we simply use polynomial interpolation, specifically we use the second barycentric form of the Chebyshev interpolant (see, for instance, Ref. [37] and references therein)

$$I_0^\alpha(E) = \sum_{j=0}^N I_0^\alpha(E(t_j)) b_j(t), \quad (\text{A15})$$

where

$$\begin{aligned} b_j(t) &= \frac{\beta_j(-1)^j}{t - t_j} \Big/ \sum_{k=0}^N \frac{\beta_k(-1)^k}{t - t_k}, \quad \text{with } \beta_j = \begin{cases} 1 & \text{if } j \neq 0, N \\ 1/2 & \text{if } j = 0, N \end{cases}, \\ E(t_j) &= \frac{t_j + 1}{2}(E_{\text{high}} - E_{\text{low}}) + E_{\text{low}}. \end{aligned}$$

with $E_{\text{high}}, E_{\text{low}}$ corresponding, respectively, to the maximum and minimum values of E for which we tabulate the integrals.

In this form the derivatives are trivially computed from

$$\frac{d}{dE} I_0^\alpha(E) = \sum_{j=0}^N b_j(t) \sum_{k=0}^N D_{jk} I_0^\alpha(E(t_k)) \quad (\text{A16})$$

where the explicit expression for the derivative matrix D can be found in section 2 of Ref. [37]. Repeated differentiation is achieved by applying the differentiation matrix multiple times. A completely analogous strategy can be employed in the case with zero external legs, allowing for an efficient determination of the integral $B_0^\alpha(E, 1)$ as well.

Appendix B: Summary of the leading non-local NLO corrections

In this appendix we summarize the main result of Ref. [32], namely the leading non-local NLO corrections that enter the effective Hamiltonian at order $\mathcal{O}(V^2)$ in the potential. Denoting this contribution by $H_{\text{eff}}^{(\text{NLO})}$, one finds

$$H_{\text{eff}}^{(\text{NLO})} = \xi H_0 + \frac{1}{2} \left[\alpha_1^{(1)} \{H_0, H_2\} + \alpha_2^{(2)} [H_0, H_2] \right] + \frac{1}{24} \left[\beta_1^{(1)} \{H_0, H_4\} + \beta_2^{(2)} [H_0, H_4] \right], \quad (\text{B1})$$

where the coefficients are given by

$$\begin{aligned} \xi &= -\frac{\lambda^2}{384(2\pi R)^2} \sum_{1234} \delta_{1+2+3+4,0} \frac{\delta(\omega_1 + \omega_2 + \omega_3 + \omega_4 - E_{\text{max}})}{\omega_1 \omega_2 \omega_3 \omega_4 (\omega_1 + \omega_2 + \omega_3 + \omega_4)}, \\ \alpha_1^{(1)} &= -\frac{\lambda^2}{48(2\pi R)^2} \sum_{123} \delta_{1+2+3,0} \frac{\delta(\omega_1 + \omega_2 + \omega_3 - E_{\text{max}})}{\omega_1 \omega_2 \omega_3 (\omega_1 + \omega_2 + \omega_3)}, \\ \alpha_2^{(2)} &= -\frac{\lambda^2}{48(2\pi R)^2} \sum_{123} \delta_{1+2+3,0} \frac{\Theta(\omega_1 + \omega_2 + \omega_3 - E_{\text{max}})}{\omega_1 \omega_2 \omega_3 (\omega_1 + \omega_2 + \omega_3)^2}, \\ \beta_1^{(1)} &= -\frac{3\lambda^2}{4\pi} \frac{1}{E_{\text{max}}^2 \sqrt{E_{\text{max}}^2 - 4m^2}}, \\ \beta_2^{(2)} &= -\frac{3\lambda^2}{64\pi R} \sum_k \frac{\Theta(2\omega_k - E_{\text{max}})}{\omega_k^4}. \end{aligned} \quad (\text{B2})$$

These expressions fully determine the NLO contribution to the effective Hamiltonian.

Appendix C: Investigating final volume effects

An interesting point to explore is the discrepancy between the correction coefficients computed in the infinite volume case (i.e. continuum momentum space) and in the finite volume case (i.e. discrete momentum space). As a case study,

we can take the part of the NLO corrections to the coupling that include a delta function. For reference, the correction is:

$$\beta_1^{(1)} = -\frac{3\lambda^2}{32\pi R} \sum_k \frac{\delta(2\omega_k - E_{\max})}{\omega_k^3}. \quad (\text{C1})$$

The continuum version of the correction reads

$$-\frac{3\lambda^2}{32\pi} F_1^3 \doteq -\frac{3\lambda^2}{32\pi} \int_{\mathbb{R}} dk \frac{\delta(2\omega(k) - E_{\max})}{\omega(k)^3}, \quad (\text{C2})$$

in this case, the constraint imposed by the delta function, $2\omega(k) = E_{\max}$, can be solved explicitly, allowing the integral to be evaluated in closed form and yielding

$$\beta_1^{(1)} = -\frac{3\lambda^2}{4\pi E_{\max}^2 \sqrt{E_{\max}^2 - 4}}. \quad (\text{C3})$$

To obtain the correction in finite volume, without losing the appropriate treatment of the delta distribution, we can translate the correction to position space. Therefore, starting from the continuum version of the correction, we can first take the Fourier transform to position space. In position space, after resolving all distributional dependencies, we can impose the finite volume. Finally, we transform back to momentum space to obtain a closed form in the now discrete momentum representation. The main idea is to write

$$\int_{\mathbb{R}} dk f(k) \delta(2\omega(k) - E_{\max}) = \int_{\mathbb{R}} dk \int dx e^{-ikx} \tilde{f}(x) \delta(2\omega(k) - E_{\max}), \quad (\text{C4})$$

where

$$\tilde{f}(x) = \int \frac{dq}{2\pi} e^{iqx} f(q). \quad (\text{C5})$$

In the specific case

$$f(k) = \frac{1}{\omega(k)^3} \Rightarrow \tilde{f}(x) = \frac{|x| K_1(|x|)}{\pi}, \quad (\text{C6})$$

where K_1 is the modified Bessel function of the second kind.

The delta function in k imposes that $k = \pm k^*$, which we can use to obtain the following representation

$$-\frac{3\lambda^2}{32\pi} \frac{E_{\max}}{2\sqrt{E_{\max}^2 - 4}} \int_{-\ell}^{\ell} dx \frac{|x| K_1(|x|)}{\pi} (e^{-ik^* x} + e^{ik^* x}) = -\frac{3\lambda^2}{4\pi E_{\max}^2 \sqrt{E_{\max}^2 - 4}} \underbrace{\left[\frac{E_{\max}^3}{4\pi} \int_0^{\ell} dx \cos(k^* x) x K_1(x) \right]}_{\hat{\beta}_1^{(1)}} \quad (\text{C7})$$

where we have defined $\ell \doteq \pi R$ and used the parity of the integrand to restrict the integration to positive values of x .

Note that, in the infinite-volume limit $\ell \rightarrow \infty$, the dimensionless factor $\hat{\beta}_1^{(1)}$ approaches 1. This implies that finite-volume effects become negligible and the finite-volume expression for $\beta_1^{(1)}$ reduces to the corresponding continuum result, consistently reproducing the correction computed in infinite volume.

Table II reports the numerical values of the finite-volume factor $\hat{\beta}_1^{(1)}$ as a function of the energy cut-off E_{\max} , for two representative choices of the spatial extent ℓ . The data illustrate how the finite-volume evaluation of the correction depends on both the volume and the UV cut-off. For the default choice $\ell = 5 \rightarrow R = 10/2\pi$, the difference between the finite-volume and infinite-volume results is sizable, and the results show a strong sensitivity to E_{\max} . In contrast, increasing to $\ell = 10 \rightarrow R = 20/2\pi$ not only smooths the dependence on the energy cut-off but also significantly reduces the discrepancy between the infinite volume and the finite volume results.

E_{\max}	$\hat{\beta}_1^{(1)}(\ell = 5)$	$\hat{\beta}_1^{(1)}(\ell = 10)$
10	0.763252	0.997042
13	1.28771	1.00476
15	0.557404	0.993781
18	1.6213	1.00943
20	0.264269	0.989269
23	2.03662	1.01543
25	-0.145361	0.983134
28	2.50951	1.02268
30	-0.697936	0.975158

TABLE II. Numerical values of the dimensionless factor $\hat{\beta}_1^{(1)}$, defined in Eq. (C7), evaluated at fixed spatial extent $\ell = \pi R$ for two representative volumes, $\ell = 5$ and $\ell = 10$, and for different values of the energy cut-off E_{\max} .

[1] K. G. Wilson, Renormalization group and critical phenomena. 2. Phase space cell analysis of critical behavior, *Phys. Rev. B* **4**, 3184 (1971).

[2] K. G. Wilson, Confinement of Quarks, *Phys. Rev. D* **10**, 2445 (1974).

[3] J. Berges, Introduction to nonequilibrium quantum field theory, *AIP Conf. Proc.* **739**, 3 (2004), arXiv:hep-ph/0409233.

[4] C. Wetterich, Exact evolution equation for the effective potential, *Phys. Lett. B* **301**, 90 (1993), arXiv:1710.05815 [hep-th].

[5] M. Creutz, Monte Carlo Study of Quantized SU(2) Gauge Theory, *Phys. Rev. D* **21**, 2308 (1980).

[6] P. de Forcrand, Simulating QCD at finite density, *PoS LAT2009*, 010 (2009), arXiv:1005.0539 [hep-lat].

[7] C. Gattringer and K. Langfeld, Approaches to the sign problem in lattice field theory, *Int. J. Mod. Phys. A* **31**, 1643007 (2016), arXiv:1603.09517 [hep-lat].

[8] J. B. Kogut and L. Susskind, Hamiltonian Formulation of Wilson's Lattice Gauge Theories, *Phys. Rev. D* **11**, 395 (1975).

[9] M. C. Bañuls and K. Cichy, Review on Novel Methods for Lattice Gauge Theories, *Rept. Prog. Phys.* **83**, 024401 (2020), arXiv:1910.00257 [hep-lat].

[10] P. Silvi, E. Rico, T. Calarco, and S. Montangero, Lattice Gauge Tensor Networks, *New J. Phys.* **16**, 103015 (2014), arXiv:1404.7439 [quant-ph].

[11] D. B. Kaplan and J. R. Stryker, Gauss's law, duality, and the Hamiltonian formulation of U(1) lattice gauge theory, *Phys. Rev. D* **102**, 094515 (2020), arXiv:1806.08797 [hep-lat].

[12] R. C. Brower, D. Berenstein, and H. Kawai, Lattice Gauge Theory for a Quantum Computer, *PoS LATTICE2019*, 112 (2020), arXiv:2002.10028 [hep-lat].

[13] V. P. Yurov and A. B. Zamolodchikov, Truncated conformal space approach to scaling lee-yang model, *Int. J. Mod. Phys. A* **5**, 3221 (1990).

[14] V. P. Yurov and A. B. Zamolodchikov, Truncated fermionic space approach to the critical 2-D Ising model with magnetic field, *Int. J. Mod. Phys. A* **6**, 4557 (1991).

[15] T. Rakovszky, M. Mestyán, M. Collura, M. Kormos, and G. Takács, Hamiltonian truncation approach to quenches in the Ising field theory, *Nucl. Phys. B* **911**, 805 (2016), arXiv:1607.01068 [cond-mat.stat-mech].

[16] P. Schmoll, J. Naumann, A. Nietner, J. Eisert, and S. Sotiriadis, Hamiltonian truncation tensor networks for quantum field theories, (2023), arXiv:2312.12506 [quant-ph].

[17] R. Houtz and J. Ingoldby, Hamiltonian Truncation Framework for Gauge Theories on the Interval, (2025), arXiv:2509.17890 [hep-th].

[18] M. Hogervorst, S. Rychkov, and B. C. van Rees, Truncated conformal space approach in d dimensions: A cheap alternative to lattice field theory?, *Phys. Rev. D* **91**, 025005 (2015), arXiv:1409.1581 [hep-th].

[19] J. Elias-Miró and E. Hardy, Exploring Hamiltonian Truncation in $d = 2 + 1$, *Phys. Rev. D* **102**, 065001 (2020), arXiv:2003.08405 [hep-th].

[20] H. Chen, A. L. Fitzpatrick, E. Katz, and Y. Xin, Giving Hamiltonian truncation a boost, *JHEP* **03**, 043, arXiv:2207.01659 [hep-th].

[21] N. Anand, A. L. Fitzpatrick, E. Katz, Z. U. Khandker, M. T. Walters, and Y. Xin, Introduction to Lightcone Conformal Truncation: QFT Dynamics from CFT Data, (2020), arXiv:2005.13544 [hep-th].

[22] A. L. Fitzpatrick and E. Katz, Snowmass White Paper: Hamiltonian Truncation, (2022), arXiv:2201.11696 [hep-th].

[23] P. Giokas and G. Watts, The renormalisation group for the truncated conformal space approach on the cylinder, (2011), arXiv:1106.2448 [hep-th].

[24] S. Rychkov and L. G. Vitale, Hamiltonian truncation study of the ϕ^4 theory in two dimensions, *Phys. Rev. D* **91**, 085011 (2015), arXiv:1412.3460 [hep-th].

- [25] S. Rychkov and L. G. Vitale, Hamiltonian truncation study of the ϕ^4 theory in two dimensions. II. The \mathbb{Z}_2 -broken phase and the Chang duality, *Phys. Rev. D* **93**, 065014 (2016), [arXiv:1512.00493 \[hep-th\]](https://arxiv.org/abs/1512.00493).
- [26] J. Elias-Miro, M. Montull, and M. Riembau, The renormalized Hamiltonian truncation method in the large E_T expansion, *JHEP* **04**, 144, [arXiv:1512.05746 \[hep-th\]](https://arxiv.org/abs/1512.05746).
- [27] J. Elias-Miro, S. Rychkov, and L. G. Vitale, NLO Renormalization in the Hamiltonian Truncation, *Phys. Rev. D* **96**, 065024 (2017), [arXiv:1706.09929 \[hep-th\]](https://arxiv.org/abs/1706.09929).
- [28] J. Elias-Miro, S. Rychkov, and L. G. Vitale, High-Precision Calculations in Strongly Coupled Quantum Field Theory with Next-to-Leading-Order Renormalized Hamiltonian Truncation, *JHEP* **10**, 213, [arXiv:1706.06121 \[hep-th\]](https://arxiv.org/abs/1706.06121).
- [29] J. Ingoldby, M. Spannowsky, T. Sypchenko, S. Williams, and M. Wingate, Real-Time Scattering on Quantum Computers via Hamiltonian Truncation, (2025), [arXiv:2505.03878 \[quant-ph\]](https://arxiv.org/abs/2505.03878).
- [30] P. Draper, L. Hidalgo, and A. Ilderton, Hamiltonian truncation and quantum simulation of strong-field QED beyond tree level, (2025), [arXiv:2509.15495 \[hep-ph\]](https://arxiv.org/abs/2509.15495).
- [31] T. Cohen, K. Farnsworth, R. Houtz, and M. A. Luty, Hamiltonian Truncation Effective Theory, *SciPost Phys.* **13**, 011 (2022), [arXiv:2110.08273 \[hep-th\]](https://arxiv.org/abs/2110.08273).
- [32] E. Demiray, K. Farnsworth, and R. Houtz, Systematic Improvement of Hamiltonian Truncation Effective Theory, (2025), [arXiv:2507.15941 \[hep-th\]](https://arxiv.org/abs/2507.15941).
- [33] O. Delouche, J. Elias Miro, and J. Ingoldby, Hamiltonian truncation crafted for UV-divergent QFTs, *SciPost Phys.* **16**, 105 (2024), [arXiv:2312.09221 \[hep-th\]](https://arxiv.org/abs/2312.09221).
- [34] J. Elias Miro and J. Ingoldby, Effective Hamiltonians and Counterterms for Hamiltonian Truncation, *JHEP* **07**, 052, [arXiv:2212.07266 \[hep-th\]](https://arxiv.org/abs/2212.07266).
- [35] J. Zinn-Justin, *From Random Walks to Random Matrices*, Oxford Graduate Texts (Oxford University Press, 2019).
- [36] https://github.com/AndreaMaestri01/HTET_Resum_NNLO (2026).
- [37] M. Diehl, R. Nagar, and F. J. Tackmann, ChiliPDF: Chebyshev interpolation for parton distributions, *Eur. Phys. J. C* **82**, 257 (2022), [arXiv:2112.09703 \[hep-ph\]](https://arxiv.org/abs/2112.09703).